First-Principles Computational Modeling of Fluorescence Resonance Energy Transfer in Co-Sensitized Dye Solar Cells

ARTICLE *in* JOURNAL OF PHYSICAL CHEMISTRY LETTERS · JULY 2012

Impact Factor: 7.46 · DOI: 10.1021/jz300839e

2 AUTHORS:

Mariachiara Pastore
Italian National Research Council
52 PUBLICATIONS **1,248** CITATIONS
SEE PROFILE

Filippo De Angelis
Università degli Studi di Perugia
265 PUBLICATIONS **11,207** CITATIONS
SEE PROFILE

THE JOURNAL OF PHYSICAL CHEMISTRY Letters

Letter

pubs.acs.org/JPCL

First-Principles Computational Modeling of Fluorescence Resonance Energy Transfer in Co-Sensitized Dye Solar Cells

Mariachiara Pastore* and Filippo De Angelis*

Computational Laboratory for Hybrid Organic Photovoltaics (CLHYO), Istituto CNR di Scienze e Tecnologie Molecolari, via Elce di Sotto 8, I-06123, Perugia, Italy

Supporting Information

ABSTRACT: TiO_2 cosensitization by different dyes having complementary absorption represents an appealing strategy to obtain panchromatic sensitization in dye-sensitized solar cells. Fluorescence (Föster) resonance energy transfer (FRET) from an energy relay dye to a sensitizing dye, both grafted onto TiO_2, was effectively shown to produce additional photocurrent (Hardin et al. *J. Am. Chem. Soc.* **2011**, *133*, 10662). Here we develop a realistic cosensitization model to provide a precise estimate of the geometrical parameters, which govern the FRET rate. The reliability of our model is fully confirmed by the quantitative reproduction of the experimental spectral shift in the naphtalocyanine absorption band and by the excellent agreement between the experimentally reported FRET rates. Our model provides a realistic picture of the cosensitized TiO_2 interface and is capable, at the same time, of predicting the cosensitization mechanism and the associated FRET kinetics based on the sole photophysical characterization of the isolated donor/acceptor partners

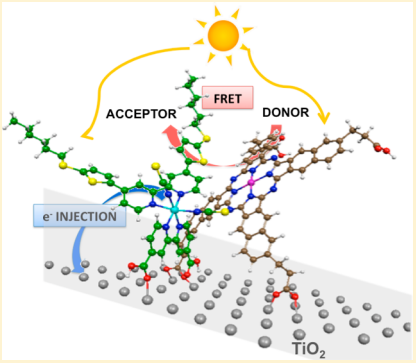

SECTION: Energy Conversion and Storage; Energy and Charge Transport

Dye-sensitized solar cells (DSCs),[1−3] offer a promising alternative to conventional silicon-based solar technologies, providing high-efficiency and reduced fabrication costs. Up to now, the highest-performance DSC devices employing liquid I^-/I_3^- electrolyte[4] are still those sensitized with Ru(II)-based dyes, such as N3, N719, or C106,[2,5] although a number of promising metal-free dyes[6,7] have been developed, with overall efficiencies approaching 10%.[8,9] In conjunction with ferrocene or cobalt-based electrolytes, organic dyes have been shown to clearly outperform Ru(II) dyes.[6,10−14]

The mixture of sensitizers having complementary absorption spectra, one of them possibly possessing high light-harvesting capability in the red and near-infrared (NIR) regions, represents an appealing strategy to obtain panchromatic TiO_2sensitization.[15−26] The design of optimal NIR sensitizers with high injection efficiency and endowed with low recombination rates of injected electrons with both electrolyte and oxidized dye is a challenging task, and until now limited DSC open-circuit voltages (V_{oc}) have been obtained,[27,28] probably due to parasitic charge-transfer processes.

An alternative approach is to use the NIR dye as an energy relay dye (ERD) (coadsorbed to the oxide surface,[23,29] tethered to the sensitizing dye (SD),[30−32] or dissolved in the electrolyte solution[29,33−36]), which remains electronically insulated from the TiO_2 surface and solely transfers its excited-state energy, via fluorescence (Föster) resonance energy transfer (FRET),[37] to the SD to produce additional photocurrent.[38] FRET is mediated by the coupling of two resonant dipoles in the presence of an electric field.[38] The geometry of the donor−acceptor system directly determines the energy transfer rate, which is given by

$$k_F = \frac{1}{\tau_0}\frac{R_0^6}{|r_A - r_D|^6} \quad (1)$$

where τ_0 is the lifetime of the donor excited state, R_0 is the Föster radius, and r_D and r_A are the position vectors of the donor and the acceptor, respectively. The Föster radius, defined as the distance between the donor and the acceptor when the FRET has 50% probability,[38] can be obtained from the donor luminescence efficiency, Q_D, the overlap integral of the donor emission spectrum, F_D, and the acceptor absorption spectrum, ε_A, and the orientation factor, κ^2

$$R_0^6 = \frac{9000 \times \ln(10)\kappa^2 Q_D}{128\pi^5 n^4 N_A}\int F_D(\lambda)\varepsilon_A(\lambda)\lambda^4\, d\lambda \quad (2)$$

where N_A is Avogadro's number and n is the refractive index of the medium. The dimensionless orientation factor κ^2 can vary from 0 to 4 and is given by

$$\kappa^2 = (\cos\gamma - 3\cos\alpha\cos\beta)^2 \quad (3)$$

where the angles α, β, and γ define the relative orientation between the two interacting dipole moments (see Scheme S1 in Supporting Information).[39] For randomly oriented dipole moments, κ^2 is equal to 2/3, but for different geometries and

Received: June 28, 2012
Accepted: July 26, 2012
Published: July 26, 2012

   dx.doi.org/10.1021/jz300839e | *J. Phys. Chem. Lett.* 2012, 3, 2146−2153

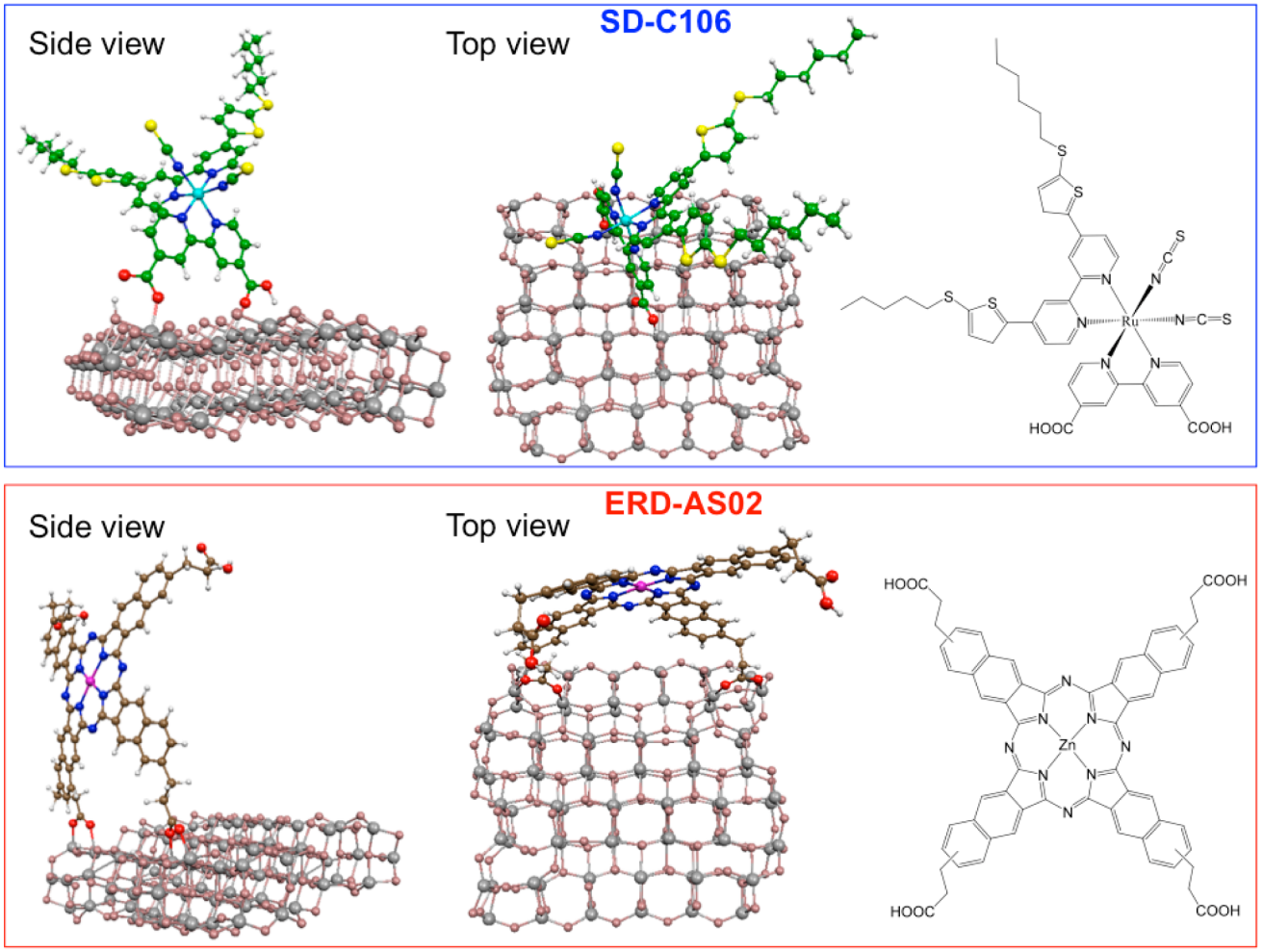

Figure 1. Side and top views and the optimized structures of C106@$(TiO_2)_{82}$ (top panel) and AS02@$(TiO_2)_{82}$ systems (bottom panel); the chemical structures of the sensitizers are also displayed.

distributions, it can be precisely calculated.[40−42] Notice that FRET modeling based on the donor/acceptor transition densities rather than simply on their dipole moments has been previously reported.[43,44] To enhance the FRET efficiency and reduce the voltage losses, a careful tuning of the electronic, optical, and structural properties of the NIR-ERD is required: (i) it should have intense absorption and high-photoluminescence quantum efficiency; (ii) its emission spectrum should largely overlap the absorption spectrum of SD; (iii) its HOMO should be lower than the redox mediator potential to have fast regeneration; and (iv) it should intimately mix, in a proper geometrical arrangement, and interact with the SD

Recently, FRET occurring from NIR-ERD to SDs has been successfully exploited in DSCs.[29,45] In particular, in a recent work, Hardin et al.[29] have reported on the energy transfer between a NIR zinc naphthalocyanine ERD (AS02) and a Ru(II) SD (C106), which are both grafted onto the TiO_2 surface to minimize the intermolecular distances and thus maximize the rate of energy transfer. To enhance the FRET and suppress the detrimental hole transfer, a proper molecular design, with the introduction of bulky groups[29,46] or selective coadsorption[47,48] is required. In this perspective, a realistic computational modeling of the sensitizer anchoring geometries and of the preferred packing schemes on the TiO_2 surface with the associated electronic coupling, optical response, and the possibility of predicting the Föster radii and the FRET rates would represent an extremely powerful tool. On the basis of our experience in the modeling of organic[49−51] and inorganic[2,52] sensitizers and of dye/TiO_2 heterointerfaces,[53−58] here we propose a first-principles density functional theory (DFT) and time-dependent (TD) DFT computational modeling of FRET occurring in cosensitized DSCs. We have calculated the adsorption mode of both AS02 and C106 on TiO_2 and then modeled the incremental cosensitization pathways, making use of the TiO_2-optimized geometries of the individual fragments. By evaluating the coupling between the transition dipole moments of the various determined ERD-SD assemblies, we computed the corresponding κ^2 values and, using these values in eq 2 along with the experimental quantities determined by Hardin et al., we obtained new estimates of the Föster radii. Having determined corrected Föster radii and exact donor−acceptor separations, we recomputed the FRET rates using the experimental fluorescence decay lifetime,[29] showing that when the energy-transfer partners are adsorbed on TiO_2, some preferential NIR-ERD/SD orientations dictated by the surface topology can lead to variation of k_{FRET} rates by two to three orders of magnitude. Our model provides us a reliable scheme of the cosensitization mechanism, the donor−acceptor distances, and the orientation factor κ^2, thus allowing the determination of the FRET kinetics based on the sole photophysical characterization of the isolated FRET partners (i.e., photoluminescence quantum efficiencies,

dx.doi.org/10.1021/jz300839e | J. Phys. Chem. Lett. 2012, 3, 2146−2153

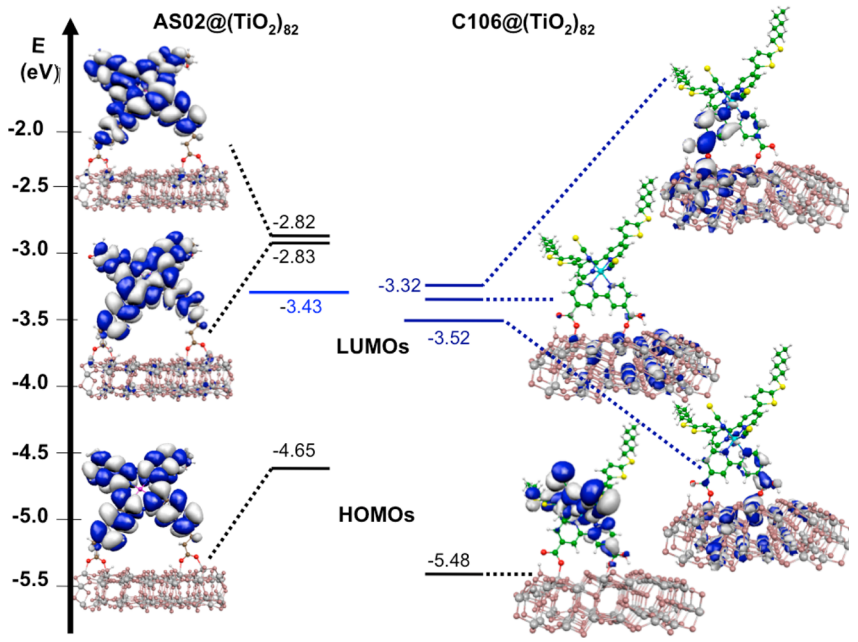

Figure 2. Alignment of the ground-state energy levels for the interacting AS02@TiO_2 (left) and C106@TiO_2 (right) systems calculated by B3LYP in water solution. Isodensity plots of the HOMO and low-lying LUMOs systems are also depicted.

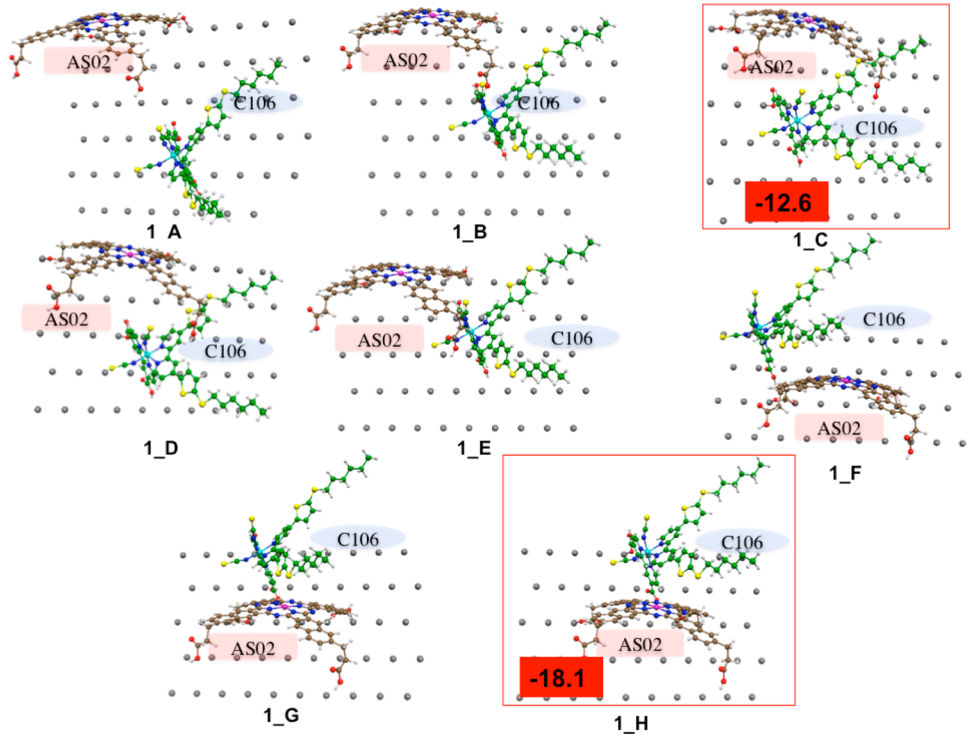

Figure 3. Top view of the 1:1 coadsorption schemes; the most stable structures are shown within red frames along with their D3-B3LYP interaction energies in vacuo (kcal/mol).

absorption and emission spectra and their overlap, fluorescence decay rate, etc.).

The optimized structures of the SD and NIR-ERD grafted onto our (101) anatase $(TiO_2)_{82}$ model along with the chemical structures of the dye molecules are displayed in Figure 1. For the C106 SD, we considered the two carboxylic groups of the anchoring bipyridine ligand to interact with Ti sites on two successive rows of penta-coordinated Ti atoms.[59] The optimized C106@$(TiO_2)_{82}$ structure has a monodentate coordination of both carboxylic groups, with one proton transferred to the surface (O_{TiO_2}-H distance of 1.07 Å) and interacting with the carboxylate via hydrogen bond (O_{C106}-H distance of 1.44 Å) and the other one retained by the dye (O_{C106}-H distance of 1.14 Å), stabilized by hydrogen-bonding with a surface oxygen (O_{TiO_2}–H distance of 1.32 Å).

Concerning AS02, one should consider both a planar binding mode with four anchoring points to the metal oxide surface,

dx.doi.org/10.1021/jz300839e | J. Phys. Chem. Lett. 2012, 3, 2146–2153

suggested for porphyrins and phtalocyanines,[60] and an "orthogonal" adsorption geometry, with the dye standing up almost perpendicular to the TiO_2 surface, with two anchoring points. Clearly, for a dye monolayer, the two adsorption modes give rise to sizably different surface coverage. With reference to the surface coverage of ~1 dye/nm^2 in ref 29, here we just consider the "orthogonal" binding mode, which is the only adsorption geometry compatible with the experimentally measured coverage.

We predict for AS02, a bidentate bridging anchoring mode of both carboxylic groups, with protons transferred to nearby surface oxygen atoms (Figure 1). Two possible anchoring orientations of AS02 have been considered, that is, the structure in Figure 1, and an alternative orientation (Supporting Information), resembling the "diagonal" orientation found for the C106 molecule. We found, however, the latter structure to be 13 to 16 kcal/mol less stable than the former one depending on the employed level of theory.

The energy level diagram of AS02@$(TiO_2)_{82}$ and C106@$(TiO_2)_{82}$ is reported in Figure 2. For AS02, we calculated a HOMO energy of −4.65 eV, to be compared with the experimental value of −4.60 eV[29] and a TiO_2 LUMO at −3.43 eV. The quasi-degenerate LUMO and LUMO+1 are only slightly mixed with unoccupied TiO_2 states, reflecting their weak coupling and are calculated at −2.83 eV. The electronic structure of C106@TiO_2 reveals the expected dye/semiconductor alignment of the energy levels,[57] with the mixed Ru-NCS HOMO (Figure 2) lying within the TiO_2 band gap and the dye virtual orbitals strongly mixing with the TiO_2 manifold of unoccupied states. We calculate the C106 HOMO at −5.48 eV, slightly overstabilized with respect to the reported value of −5.27 eV[61] determined in the gas phase; the TiO_2 conduction band edge, partially overlapped with the dye LUMOs levels, is calculated at −3.52 eV, close to the value obtained for AS02@TiO_2. The LUMO with large components on C106 is calculated at −3.32 eV, that is, 0.2 eV above the lowest unoccupied semiconductor state.[55]

We have investigated the stability of various coadsorption patterns, from AS02:C106 1:1 aggregates (Figure 3) to 1:4 ones (Supporting Information). The interaction energies, given by the difference between the total energy of the aggregate structures and the sum of the energies of its noninteracting components, for all of the investigated systems are reported in Supporting Information; here we just report the energetics for the most stable assemblies. We label the aggregate structures as *n*_X, with *n* ranging from 1 to 4 representing the number of SDs surrounding the ERD and X (A-D) representing the different investigated interaction patterns. The most stable aggregate 3_X and 4_X structures (3_D and 4_B) are displayed in Figures 4.

On the technical side, we note the different interaction energies obtained by B3LYP and D3-B3LYP;[56] the inclusion of the D3 correction, accounting for dispersion interactions, provides a coherent trend within the calculated values, with an interaction energy increasing as the number of SD molecules increases, with the only exception of the 1:2 structure (Supporting Information), given by combining the most stable 1_C and 1_H 1:1 (SD:ERD) assemblies, which turns out to be less stable than both of the constituent 1:1 structures, due to a repulsive interaction between the two C106 molecules.

Moving to the 1:3 cosensitization patterns (Supporting Information), we find three assemblies (3_A, 3_C, and 3_D) with a stabilization energy close to −27 kcal/mol and relative

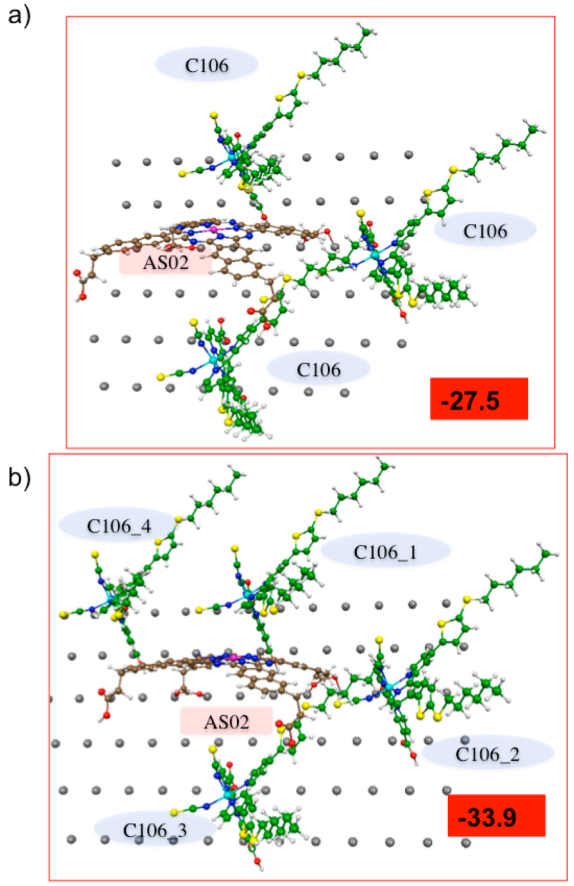

Figure 4. Top view of the most stable 1:3 coadsorption scheme 3_D (a) and of the 1:4 one 4_B (b) and their D3-B3LYP interaction energies in vacuo (kcal/mol); in the latter, representing the final coadsorption pattern, the numbering order of the C106 molecules is also reported.

differences within 1 kcal/mol; the most stable 3_D aggregate is shown in Figure 4. For the 1:4 aggregates, the 4_B structure (Figure 4) is the most stable one, with a B3LYP-D3 stabilization energy of −34 kcal/mol.

To compare the calculated absorption spectra of the isolated molecules and those of the aggregate structures, we present TDDFT results obtained on the isolated dyes at their optimized geometries of the adsorbed species. Using the TiO_2-adsorbed geometries, for the isolated AS02 and C106 in solution, we calculated absorption maxima at 766 and 531 nm, respectively (see Figure 5, red and blue lines, respectively), which nicely reproduce the experimentally measured absorption peaks located at 773 (AS02) and 550 nm (C106).[29] We also carried out reference TDDFT calculations employing the optimized geometries of the isolated dyes, obtaining essentially coincident absorption maxima (766 and 530 nm for AS02 and C106, respectively). Optimizing the geometry of the S1 state of AS02 by TDDFT (B3LYP/6-31G*), we calculated an emission wavelength of 779 nm, in excellent agreement with the experimental emission peak recorded at 782 nm.[29]

The experimental absorption spectra of the cosensitized TiO_2 (ca. 1:4 AS02:C106 ratio) showed a slight red-shifting and a small intensity decreasing of the AS02 absorption peak.[29] This spectral shift was attributed to a weak electronic interaction between the SD and ERD occurring for the TiO_2-anchored systems.[29] As shown in Figure 5, comparing the

dx.doi.org/10.1021/jz300839e | J. Phys. Chem. Lett. 2012, 3, 2146−2153

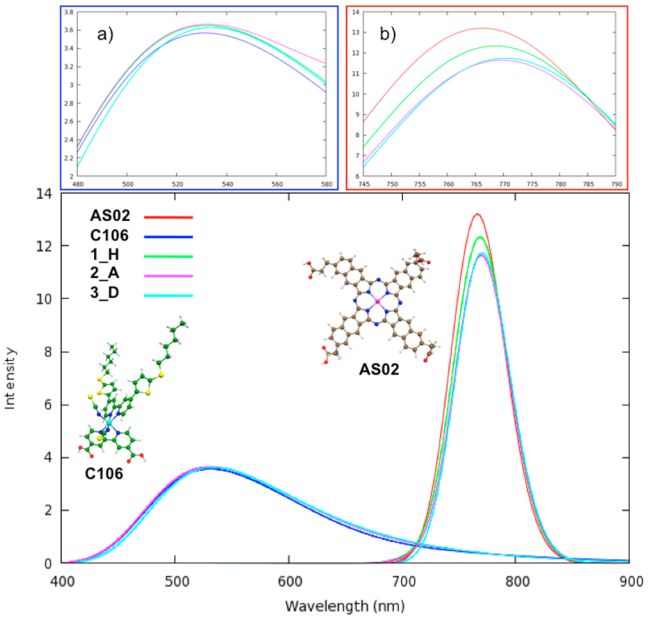

Figure 5. Bottom: Calculated absorption spectra in water of isolated AS02 (red line) and C106 (blue line) sensitizers as well as of the 1_H (light green line), 2_A (magenta line), and 3_D (cyano line) configurations. Top: the two insets report the band maxima shifts for C106 (a) and AS02 (b). The spectra of C106 and AS02 have been simulated by a Gaussian broadening with σ = 0.05 and 0.20 eV, respectively. To reproduce the experimental ratio between the C106 and AS02 extinction coefficients of about 1:5, we multiplied the computed intensities of C106 by a factor of five.

TDDFT simulated spectrum of the isolated AS02 to those of the 1_H, 2_A, and 3_D cosensitized structures, we progressively reproduce the small red shift and the intensity decrease in the ERD absorption band. For 3_D, we calculate an adsorption maximum of 770 nm, to be compared with the 766 nm value obtained for the isolated ERD. Having reproduced the spectral response associated with the formation of coadsorbed AS02-C106 monolayer, we are confident that our model provides a realistic picture of the SD/ERD interactions and cosensitization pattern on TiO_2.

Assuming κ^2 = 2/3, a Foster radius (R_0) for energy transfer from AS02 to C106 in the range of 1.5 to 1.8 nm was calculated by Hardin et al.[29] (Table 1). As pointed out by the authors, this value should be taken as an average estimate of the actual R_0 because both dyes are anchored to the titania surface with precise orientations of their transition dipole moments. On the basis of surface coverage measurements, an average separation between the ERD and SD of ∼1 nm (i.e., 0.914 nm) was estimated.[29] These data, together with the AS02 natural fluorescence decay lifetime and measured spectral overlap, provided FRET rates between 7.1 × 10^9 and 2.3 × 10^{10} s^{-1} (Table 1), considering the lower and upper bound to R_0, respectively.[29]

Our cosensitization model (Supporting Information) provides us with all of the required geometrical and electronic parameters, which are not directly accessible from experimental measurements. To proceed with the calculation of the κ^2 orientation factor, we define the vector distance between the donor and acceptor ground-to-excited transition dipole moments as the distance between the centers of nuclear charges (r_{DA}) for each AS02-C106 couple; see Table 1. For the AS02 transition dipole moment, we took the averaged dipole moments of the two near-degenerate S1 and S2 transitions[39] (Supporting Information). The r_{DA} values are roughly comparable to the calculated distances between the metal centers, Ru and Zn (r_{Ru-Zn}), Table 1. Using eq 3, we have computed for each D−A geometry the value of κ^2 (the calculated values of α, β, and γ are listed in the Supporting Information) and recalculated the Foster radii, R'_0, by correcting the values reported by Hardin et al.[29] with our calculated κ^2. The shortest separations are predicted for the AS02-C106_1 (1.027 nm) and AS02-C106_3 (1.054 nm) D−A couples, Figure 4b, which are also the structures with the largest stabilization energies (−18.1 and −12.6 kcal/mol, respectively) and the largest κ^2 values, 1.46 and 0.54, respectively. For the AS02-C106_2 and AS02-C106_4 D−A structures, Figure 4b, we obtained considerably smaller κ^2 values, 0.08 and 0.15, and longer intermolecular distances of 1.680 and 1.495 nm, respectively. The κ^2 values reported in Table 1, and consequently the Föster radii and their sixth power, $R'_0{}^6$, substantially differ from the values used in ref 29 to estimate the FRET rate. Here the largest calculated κ^2 value is 1.46, more than two times larger than the value of 2/3 valid in solution, and the corrected FRET radius is between 1.7 and 2.1 nm, again larger than the 1.5 to 1.8 nm range reported by Hardin et al.; the smallest κ^2 value is instead 0.08 (AS02-C106_2), with corresponding Föster radii of 1.1 to 1.3 nm. With reference to eq 1, it is clear that the small differences in the calculated FRET radii become very relevant because the

Table 1. Calculated Interaction Energies, E_{int} (kcal/mol), Charge Center and Ru−Zn Distances (nm), κ^2 and Corresponding Corrected R'_0, $R'_0{}^6$ (in nm), and FRET Rates, k'_{FRET}, for Each AS02-C106 D-A Couple[a]

D−A couple	E_{int} (kcal/mol)	$\lvert r_{DA}\rvert$ (nm)	$\lvert r_{Ru-Zn}\rvert$ (nm)	κ^2	R'_0 (nm)	$R'_0{}^6$ (nm^6)	k'_{FRET} (s^{-1})
AS02-C106_1	−18.1	1.027	0.908	1.46	1.7	24.1	7.5 × 10^9
					2.1	85.8	2.7 × 10^{10}
AS02-C106_2	−3.8	1.680	1.416	0.08	1.1	1.8	2.9 × 10^7
					1.3	4.8	7.8 × 10^7
AS02-C106_3	−12.6	1.054	1.221	0.53	1.4	7.5	2.0 × 10^9
					1.7	24.1	6.4 × 10^9
AS02-C106_4	−1.4	1.495	1.702	0.15	1.2	3.0	9.8 × 10^7
					1.4	7.5	2.4 × 10^8
experiment[29]		0.914		0.67	1.5	11.4	7.1 × 10^9
					1.8	34.0	2.3 × 10^{10}

[a]Couples labeling is illustrated in Figure 4b and S5 in the Supporting Information. The last row reports the corresponding experimental values taken from ref 29.

dx.doi.org/10.1021/jz300839e | J. Phys. Chem. Lett. 2012, 3, 2146−2153

corrected $R'_0{}^6$ values vary from 1.8 to 85.8 nm^6. In Table 1, we report our estimates of the FRET rates (k'_{FRET}) for each D−A couple, calculated by eq 1 using the experimental fluorescence decay lifetime of 2.75 ns[29] and the corrected R'_0 and $|r_{DA}|$ values obtained in this work. For the most interacting D−A couple (AS02-C106_1), we predicted a FRET rate between 7.5×10^9 and 2.7×10^{10} s^{-1}, which is notably *numerically the same value* obtained in ref 29. (See Table 1.) In other words, we calculate a shorter D−A separation *and* a shorter Föster radius than in ref 29, obtaining the same $R_0/|r_{DA}|$ ratio and thus obtaining the same FRET rates, being proportional to the sixth power of the above-mentioned ratio. The calculated rates in Table 1 show that unfavorable ERD-SD orientations with very low κ^2 values and large distances, like for instance the AS02-C106_2 couple, yield a sizable reduction in the FRET rates, up to three orders of magnitude.

We incidentally remark that our model also provides an estimate of the electronic coupling for hole transfer from the SD to the NIR-ERD. As an example, for the most interacting AS02-C106_1 configuration, Figure 4b, we calculate a rather small electronic coupling of $\sim 10^{-3}$ eV. Thus one can scrutinize and possibly control at the same time both FRET and hole transfer processes, which constitute a dead end for the DSCs functioning in the present architecture.

In conclusion, we have developed a realistic cosensitization model and an accurate computational protocol capable of providing a precise estimate of the geometrical parameters, which govern the FRET rate. The reliability of our TiO_2 coadsorption scheme is fully confirmed by the quantitative reproduction of the experimental spectral shift in the ERD absorption band and by the excellent agreement between the experimental FRET rates reported in ref 29 and those predicted on the basis of our corrected κ^2, Föster radii, and donor−acceptor distances. The agreement between our modeled k_{FRET} and those experimentally estimated definitely demonstrates the reliability of the developed cosensitized TiO_2 model, which is capable, at the same time, of predicting the cosensitization mechanism and the associated FRET kinetics based on the sole photophysical characterization of the isolated FRET partners.

Our results illustrate that tuning of the FRET process in DSCs is effectively possible by judicious selection of donor−acceptor partners having the right electronic and geometrical requisites, with our unprecedented study providing the required computational modeling background to further optimize this important efficiency enhancement direction.

METHOD, MODEL AND COMPUTATIONAL DETAILS

To model the coadsorption patterns, here we have extended and refined the approach previously setup to investigate dye aggregation on titania.[56] The strategy we employ can be summarized in the following steps:

(a) Determining the adsorption geometry and the energy level alignment of the AS02 and C106 dyes on TiO_2 by performing full geometry optimizations of the dyes attached to TiO_2, followed by single-point calculations in solution.

(b) Keeping fixed the geometries of the TiO_2-adsorbed dyes, selecting among all of the possible 1:1, 1:2, 1:3 and 1:4 AS02:C106 coadsorption arrangements, the closest interacting ones with no explicit superposition of atomic structures on a grid of Ti atoms.

(c) Determining the most stable interacting configurations by performing single-point B3LYP energy evaluation with the DGDZVP basis set corrected by dispersion contributions (B3LYP-D3)[55,62,63] and simulating the optical response of the so-determined aggregates in solution by TDDFT.

(d) For the 1:4 ERD:SD coadsorption pattern, calculating for each AS02-C106 couple, composing the selected configuration, the donor−acceptor distance, the orientation parameter κ^2, given by the interaction between the transition dipole moments of AS02 and C106,[39] the corrected Föster radius, R_0, and finally, the corresponding energy transfer rate k_{FRET}.

Our TiO_2 model is a $(TiO_2)_{82}$ cluster, obtained by appropriately "cutting" an anatase slab, exposing the majority (101) surface.[64] Following the work by Persson et al.,[65] we consider a neutral stoichiometric TiO_2 cluster with no saturating atoms or groups at the cluster border. The employed $(TiO_2)_{82}$ model is an almost square TiO_2 (101) two-layer anatase slab of ∼2 nm side, with three rows of five- and six-coordinated surface Ti sites. The geometry optimizations of AS02@$(TiO_2)_{82}$ and C106@$(TiO_2)_{82}$ were carried out in gas phase with the ADF program package[66] employing the Becke−Perdew exchange-correlation functional[67,68] with a TZP/DZ basis set for Ti, Zn, Ru/H, C, N, O, and S. For the optimized dye@TiO_2 structures, the energy-level alignments have been evaluated at the B3LYP[69]/6-31G*-3-21G*(Ru) level of theory taking into account solvation effects by means of the conductor-like polarizable continuum model (C-PCM).[70,71] as implemented in the Gaussian 09 package.[72]

The TDDFT calculations on the selected configurations were carried out using the B3LYP functional and the DGDZVP basis. For AS02, we also calculated the $S_1 \rightarrow S_0$ transition carrying out the excited-state geometry optimization in gas phase with the B3LYP functional and a 6-31G* basis set.

ASSOCIATED CONTENT

Supporting Information

Optimized structure of the AS02@TiO_2 system in the alternative "diagonal" configuration; details of the coadsorption schemes selection and top views of the 2_A, 3_X, and 4_X coadsorption patterns and corresponding interaction energies; scheme of the relative orientation of the AS02 and C106 dipole moments in the 4_B coadsorption pattern and their values; and calculated values of the angle α, β, and γ for each AS02-C106 couple. This material is available free of charge via the Internet at http://pubs.acs.org.

AUTHOR INFORMATION

Corresponding Author

*E-mail: chiara@thch.unipg.it, filippo@thch.unipg.it.

Notes

The authors declare no competing financial interest.

ACKNOWLEDGMENTS

We thank FP7-NMP-2009 project 246124 "SANS", Fondazione Istituto Italiano di Tecnologia, Platform Computation, Project Seed 2009 "HELYOS" and CNR-EFOR for financial support.

REFERENCES

(1) O'Regan, B.; Grätzel, M. A Low-Cost, High-Efficiency Solar Cell Based on Dye-Sensitized Colloidal TiO_2 Films. *Nature* **1991**, *353*, 737−740.

(2) Nazeeruddin, M. K.; De Angelis, F.; Fantacci, S.; Selloni, A.; Viscardi, G.; Liska, P.; Ito, S.; Takeru, B.; Grätzel, M. Combined Experimental and DFT-TDDFT Computational Study of Photoelectrochemical Cell Ruthenium Sensitizers. *J. Am. Chem. Soc.* **2005**, *127*, 16835−16847.

(3) Grätzel, M. Recent Advances in Sensitized Mesoscopic Solar Cells. *Acc. Chem. Res.* **2009**, *42*, 1788−1798.

(4) Boschloo, G.; Hagfeldt, A. Characteristics of the Iodide/Triiodide Redox Mediator in Dye-Sensitized Solar Cells. *Acc. Chem. Res.* **2009**, *42*, 1819−1826.

(5) Grätzel, M. Conversion of Sunlight to Electric Power by Nanocrystalline Dye-Sensitized Solar Cells. *J. Photochem. Photobiol., A* **2004**, *164*, 3−14.

(6) Bai, Y.; Zhang, J.; Zhou, D.; Wang, Y.; Zhang, M.; Wang, P. Engineering Organic Sensitizers for Iodine-Free Dye-Sensitized Solar Cells: Red-Shifted Current Response Concomitant with Attenuated Charge Recombination. *J. Am. Chem. Soc.* **2011**, *133*, 11442−11445.

(7) Zhang, M.; Liu, J.; Wang, Y.; Zhou, D.; Wang, P. Redox Couple Related Influences of p-Conjugation Extension in Organic Dye-Sensitized Mesoscopic Solar Cells. *Chem. Sci.* **2011**, *2*, 1401−1406.

(8) Ito, S.; Miura, H.; Uchida, S.; Takata, M.; Sumioka, K.; Liska, P.; Comte, P.; Pechy, P.; Grätzel, M. High-Conversion-Efficiency Organic Dye-Sensitized Solar Cells with a Novel Indoline Dye. *Chem. Commun.* **2008**, 5194−5196.

(9) Zeng, W.; Cao, Y.; Bai, Y.; Wang, Y.; Shi, Y.; Zhang, M.; Wang, F.; Pan, C.; Wang, P. Efficient Dye-Sensitized Solar Cells with an Organic Photosensitizer Featuring Orderly Conjugated Ethylenedioxythiophene and Dithienosilole Blocks. *Chem. Mater.* **2010**, *22*, 1915−1925.

(10) Daeneke, T.; Kwon, T.-H.; Holmes, A. B.; Duffy, N. W.; Bach, U.; Spiccia, L. High-Efficiency Dye-Sensitized Solar Cells with Ferrocene-based electrolytes. *Nat. Chem.* **2011**, *3*, 213−217.

(11) Feldt, S. M.; Gibson, E. A.; Gabrielsson, E.; Sun, L.; Boschloo, G.; Hagfeldt, A. Design of Organic Dyes and Cobalt Polypyridine Redox Mediators for High-Efficiency Dye-Sensitized Solar Cells. *J. Am. Chem. Soc.* **2010**, *132*, 16714−16724.

(12) Feldt, S. M.; Cappel, U. B.; Johansson, E. M. J.; Boschloo, G.; Hagfeldt, A. Characterization of Surface Passivation by Poly(methylsiloxane) for Dye-Sensitized Solar Cells Employing the Ferrocene Redox Couple. *J. Phys. Chem. C* **2010**, *114*, 10551−10558.

(13) Cameron, P. J.; Peter, L. M.; Zakeeruddin, S. M.; Grätzel, M. Electrochemical Studies of the Co(III)/Co(II)(dbbip)2 Redox Couple as a Mediator for Dye-Sensitized Nanocrystalline Solar Cells. *Coord. Chem. Rev.* **2004**, *248*, 1447−1453.

(14) Yella, A.; Lee, H.-W.; Tsao, H. N.; Yi, C.; Chandiran, A. K.; Nazeeruddin, M. K.; Diau, E. W.-G.; Yeh, C.-Y.; Grätzel, M. Porphyrin-Sensitized Solar Cells with Cobalt (II/III)−Based Redox Electrolyte Exceed 12% Efficiency. *Science* **2011**, *4*, 629−634.

(15) Clifford, J. N.; Forneli, A.; Chen, H.; Torres, T.; Tan, S.; Palomares, E. Co-Sensitized DSCs: Dye Selection Criteria for Optimized Device Voc and Efficiency. *J. Mater. Chem.* **2011**, *21*, 1693−1696.

(16) Sayama, K.; Tsukagoshi, S.; Mori, T.; Hara, K.; Ohga, Y.; Shinpou, A.; Abe, Y.; Suga, S.; Arakawa, H. Efficient Sensitization of Nanocrystalline TiO_2 Films with Cyanine and Merocyanine Organic Dyes. *Sol. Energy Mater. Sol. Cells* **2003**, *80*, 47−71.

(17) Martínez-Díaz, M. V.; de la Torre; Torres, T. Lighting Porphyrins and Phthalocyanines for Molecular Photovoltaics. *Chem Commun.* **2010**, *46*, 7090−7108.

(18) Chen, Y.; Zeng, Z.; Li, C.; Wang, W.; Wang, X.; Zhang, B. Highly Efficient Co-Sensitization of Nanocrystalline TiO_2 Electrodes with Plural Organic Dyes. *New. J. Chem.* **2005**, *29*, 773−776.

(19) Yum, J.-H.; Jang, S.-R.; Walter, P.; Geiger, T.; Nüesch, F.; Kim, S.; Ko, J.; Grätzel, M.; Nazeeruddin, M. K. Efficient Co-Sensitization of Nanocrystalline TiO_2 Films by Organic Sensitizers. *Chem. Commun.* **2007**, 4680−4682.

(20) Lan, C.-M.; Wu, H.-P.; Pan, T.-Y.; Chang, C.-W.; Chao, W.-S.; Chen, C.-T.; Wang, C.-L.; Lin, C.-Y.; Diau, E. W.-G. Enhanced Photovoltaic Performance with Co-Sensitization of Porphyrin and an Organic Dye in Dye-Sensitized Solar Cells. *Energy Environ. Sci.* **2012**, *5*, 6460−6464.

(21) Yum, J.-H.; Baranoff, E.; Wenger, S.; Nazeeruddin, M. K.; Grätzel, M. Panchromatic Engineering for Dye-Sensitized Solar Cells. *Energy Environ. Sci.* **2011**, *4*, 842−857.

(22) Brown, M. D.; Parkinson, P.; Torres, T.; Miura, H.; Herz, L. M.; Snaith, H. J. Surface Energy Relay Between Cosensitized Molecules in Solid-State Dye-Sensitized Solar Cells. *J. Phys. Chem. C* **2011**, *115*, 23204−23208.

(23) Siegers, C.; Würfel, U.; Zistler, M.; Gores, H.; Hohl-Ebinger, J.; Hinsch, A.; Haag, R. Overcoming Kinetic Limitations of Electron Injection in the Dye Solar Cell via Coadsorption and FRET. *Chem. Phys. Chem.* **2008**, *9*, 793−798.

(24) Clifford, J. N.; Palomares, E.; Nazeeruddin, M. K.; Thampi, R.; Grätzel, M.; Durrant, J. R. Multistep Electron Transfer Processes on Dye Co-Sensitized Nanocrystalline TiO_2 Films. *J. Am. Chem. Soc.* **2004**, *126*, 5670−5671.

(25) Fan, S.-Q.; Kim, C.; Fang, B.; Liao, K.-X.; Yang, G.-J.; Li, C.-J.; Kim, J.-J.; Ko, J. Improved Efficiency of over 10% in Dye-Sensitized Solar Cells with a Ruthenium Complex and an Organic Dye Heterogeneously Positioning on a Single TiO_2 Electrode. *J. Phys. Chem. C* **2011**, *115*, 7747−7754.

(26) Ogura, R. Y.; Nakane, S.; Morooka, M.; Orihashi, M.; Suzuki, Y.; Noda, K. High-Performance Dye-Sensitized Solar Cell with a Multiple Dye System. *Appl. Phys. Lett.* **2009**, *94*, 073308.

(27) Macor, L.; Fungo, F.; Tempesti, T.; Durantini, E. N.; Otero, L.; Barea, E. M.; Fabregat-Santiago, F.; Bisquert, J. Near-IR Sensitization of Wide Band Gap Oxide Semiconductor by Axially Anchored Si-Naphthalocyanines. *Energy Environ. Sci.* **2009**, *2*, 529−534.

(28) Ono, T.; Yamaguchi, T.; Arakawa, H. Study on Dye-Sensitized Solar Cell Using Novel Infrared Dye. *Sol. Energy Mater. Sol. Cells* **2009**, *93*, 831−835.

(29) Hardin, B. E.; Sellinger, A.; Moehl, T.; Humphry-Baker, R.; Moser, J.-E.; Wang, P.; Zakeeruddin, S. M.; Grätzel, M.; McGehee, M. D. Energy and Hole Transfer between Dyes Attached to Titania in Cosensitized Dye-Sensitized Solar Cells. *J. Am. Chem. Soc.* **2011**, *133*, 10662−10667.

(30) Warnan, J.; Pellegrin, Y.; Blart, E.; Odobel, F. Supramolecular Light Harvesting Antennas to Enhance Absorption Cross-Section in Dye-Sensitized Solar Cells. *Chem Commun* **2012**, *48*, 675−677.

(31) Cheon, J. H.; Ah Kim, S.; Ahn, K.-S.; Kang, M.-S.; Kim, J. H. Enhanced Light-Harvesting Efficiency by Förster Resonance Energy Transfer in Quasi-Solid State DSSC Using Organic Blue Dye. *Electrochim. Acta* **2012**, *68*, 240−245.

(32) Siegers, C.; Hohl-Ebinger, J.; Zimmermann, B.; Würfel, U.; Mülhaupt, R.; Hinsch, A.; Haag, R. A Dyadic Sensitizer for Dye Solar Cells with High Energy-Transfer Efficiency in the Device. *Chem. Phys. Chem.* **2007**, *8*, 1548−1556.

(33) Hardin, B. E.; Hoke, E. T.; Armstrong, P. B.; Yum, J.-H.; Comte, P.; Torres, T.; Fréchet, J. M. J.; Nazeeruddin, M. K.; Grätzel, M.; McGehee, M. D. Increased Light Harvesting in Dye-Sensitized Solar Cells with Energy Relay Dyes. *Nat. Photonics* **2009**, *3*, 406−411.

(34) Hardin, B. E.; Yum, J.-H.; Hoke, E. T.; Jun, Y. C.; Péchy, P.; Torres, T.; Brongersma, M. L.; Nazeeruddin, M. K.; Grätzel, M.; McGehee, M. D. High Excitation Transfer Efficiency from Energy Relay Dyes in Dye-Sensitized Solar Cells. *Nano Lett.* **2010**, *10*, 3077−3083.

(35) Yum, J.-H.; Hardin, B. E.; Moon, S.-J.; Baranoff, E.; Nüesch, F.; McGehee, M. D.; Grätzel, M.; Nazeeruddin, M. K. Panchromatic Response in Solid-State Dye-Sensitized Solar Cells Containing Phosphorescent Energy Relay Dyes. *Angew. Chem., Int. Ed.* **2009**, *48*, 9277−9280.

(36) Yum, J.-H.; Hardin, B. E.; Hoke, E. T.; Baranoff, E.; Zakeeruddin, S. M.; Nazeeruddin, M. K.; Torres, T.; McGehee, M.

D.; Grätzel, M. Incorporating Multiple Energy Relay Dyes in Liquid Dye- Sensitized Solar Cells. *Chem. Phys. Chem.* **2011**, *12*, 657−661.
(37) Föster, T. 10th Spiers Memorial Lecture. Transfer Mechanisms of Electronic Excitation. *Discuss. Faraday Soc.* **1959**, *27*, 7−17.
(38) Hoke, E. T.; Hardin, B. E.; McGehee, M. D. Modeling the Efficiency of Förster Resonant Energy Transfer from Energy Relay Dyes in Dye-Sensitized Solar Cells. *Opt. Express* **2010**, *18*, 3893−3904.
(39) Mårtensson, J. Calculation of the Förster Orientation Factor for Donor-Acceptor Systems with One Chromophore of Threefold or Higher Symmetry: Zinc Porphyrin. *Chem. Phys. Lett.* **1994**, *229*, 449−456.
(40) Blumen, A.; Klafter, J.; Zumofen, G. Influence of Restricted Geometries on the Direct Energy Transfer. *J. Chem. Phys.* **1986**, *84*, 1397−1401.
(41) Drake, J.; Klafter, J.; Levitz, P. Chemical and Biological Microstructures as Probed by Dynamic Processes. *Science* **1991**, *251*, 1574−1579.
(42) Calzaferri, G.; Lutkouskaya, K. Mimicking the Antenna System of Green Plants. *Photochem. Photobiol. Sci.* **2008**, *7*, 879−910.
(43) Iozzi, M. F.; Mennucci, B.; Tomasi, J.; Cammi, R. Excitation Energy Transfer (EET) Between Molecules in Condensed Matter: A Novel Application of the Polarizable Continuum Model (PCM). *J. Chem. Phys.* **2004**, *120*, 7029.
(44) Speelman, A. L.; Muñoz-Losa, A.; Hinkle, K. L.; VanBeek, D. B.; Mennucci, B.; Kruege, B. P. Using Molecular Dynamics and Quantum Mechanics Calculations To Model Fluorescence Observables. *J. Phys. Chem. A* **2011**, *115*, 3997−4008.
(45) Shankar, K.; Feng, X.; Grimes, C. A. Enhanced Harvesting of Red Photons in Nanowire Solar Cells: Evidence of Resonance Energy Transfer. *ACS Nano* **2009**, *3*, 788−794.
(46) Kimura, M.; Nomoto, H.; Masaki, N.; Mori, S. Dye Molecules for Simple Co-Sensitization Process: Fabrication of Mixed-Dye-Sensitized Solar Cells. *Angew. Chem., Int. Ed.* **2012**, *51*, 17.
(47) Lee, K.; Park, S. W.; Ko, M. J.; Kim, K.; Park, N.-G. Selective Positioning of Organic Dyes in a Mesoporous Inorganic Oxide Film. *Nat. Mater.* **2009**, *8*, 665−671.
(48) Choi, H.; Kim, S.; Kang, S. O.; Ko, J.; Kang, M.-S.; Clifford, J. N.; Forneli, A.; Palomares, E.; Nazeeruddin, M. K.; Grätzel, M. Stepwise Cosensitization of Nanocrystalline TiO_2 Films Utilizing Al2O3 Layers in Dye-Sensitized Solar Cells. *Angew. Chem.* **2008**, *120*, 8383−8387.
(49) Pastore, M.; Mosconi, E.; De Angelis, F.; Grätzel, M. A Computational Investigation of Organic Dyes for Dye-Sensitized Solar Cells: Benchmark, Strategies, and Open Issues. *J. Phys. Chem. C* **2010**, *114*, 7205−7212.
(50) Pastore, M.; Fantacci, S.; De Angelis, F. Ab Initio Determination of Ground and Excited State Oxidation Potentials of Organic Chromophores for Dye-Sensitized Solar Cells. *J. Phys. Chem. C* **2010**, *114*, 22742−22750.
(51) Pastore, M.; Mosconi, E.; Fantacci, S.; De Angelis, F. Computational Investigations on Organic Sensitizers for Dye-Sensitized Solar Cells. *Curr. Org. Synth.* **2012**, *9*, 215−232.
(52) Fantacci, S.; De Angelis, F.; Selloni, A. Absorption Spectrum and Solvatochromism of the [Ru(4,4′-COOH-2,2′-bpy)2(NCS)2] Molecular Dye by Time Dependent Density Functional Theory. *J. Am. Chem. Soc.* **2003**, *125*, 4381−4387.
(53) Pastore, M.; De Angelis, F. Computational Modeling of Stark Effects in Organic Dye-Sensitized TiO_2 Heterointerfaces. *J. Phys. Chem. Lett.* **2011**, *2*, 1261−1267.
(54) Pastore, M.; De Angelis, F. Computational Modelling of TiO_2 Surfaces Sensitized by Organic Dyes With Different Anchoring Groups: Adsorption Modes, Electronic Structure and Implication for Electron Injection/Recombination. *Phys. Chem. Chem. Phys.* **2012**, *14*, 920−928.
(55) Pastore, M.; Mosconi, E.; De Angelis, F. Computational Investigation of Dye−Iodine Interactions in Organic Dye-Sensitized Solar Cells. *J. Phys. Chem. C* **2012**, *116*, 5965−5973.
(56) Pastore, M.; De Angelis, F. Aggregation of Organic Dyes on TiO_2 in Dye-Sensitized Solar Cells Models: An Ab Initio Investigation. *ACS Nano* **2010**, *4*, 556−562.
(57) De Angelis, F.; Fantacci, S.; Mosconi, E.; Nazeeruddin, M. K.; Grätzel, M. Absorption Spectra and Excited State Energy Levels of the N719 Dye on TiO_2 in Dye-Sensitized Solar Cell Models. *J . Phys. Chem. C* **2011**, *115*, 8825−8831.
(58) De Angelis, F. Direct vs. Indirect Injection Mechanisms in Perylene Dye-Sensitized Solar Cells: A DFT/TDDFT Investigation. *Chem. Phys. Lett.* **2010**, *493*, 323−327.
(59) Labat, F.; Adamo, C. Bi-isonicotinic Acid on Anatase (101): Insights from Theory. *J. Phys. Chem. C* **2007**, *111*, 15034−15042.
(60) Li, X.; Wang, H.; Wu, H. Phthalocyanines and Their Analogs Applied in Dye-Sensitized Solar Cell. In *Functional Phthalocyanine Molecular Materials*; Springer: Berlin, 2010; Vol. *135*, pp 229−273.
(61) Cao, Y.; Bai, Y.; Yu, Q.; Cheng, Y.; Liu, S.; Shi, D.; Gao, F.; Wang, P. Dye-Sensitized Solar Cells with a High Absorptivity Ruthenium Sensitizer Featuring a 2-(Hexylthio)thiophene Conjugated Bipyridine. *J. Phys. Chem. C* **2009**, *113*, 6290−62−97.
(62) Grimme, S.; Ehrlich, S.; Goerigk, L. Effect of the Damping Function in Dispersion Corrected Density Functional Theory. *J. Comput. Chem.* **2011**, *32*, 1456−1465.
(63) Grimme, S.; Antony, J.; Ehrlich, S.; Krieg, H. A Consistent and Accurate Ab Initio Parametrization of Density Functional Dispersion Correction (DFT-D) for the 94 Elements H-Pu. *J. Chem. Phys.* **2010**, *132*, 154104.
(64) Vittadini, A.; Selloni, A.; Rotzinger, F. P.; Grätzel, M. Structure and Energetics of Water Adsorbed at TiO_2 Anatase (101) and (001) Surfaces. *Phy. Rev. Lett.* **1998**, *81*, 2954−2957.
(65) Lundqvist, M. J.; Nilsing, M.; Persson, P.; Lunel, S. DFT Study of Bare and Dye-Sensitized TiO_2 Clusters and Nanocrystals. *Int. J. Quantum Chem.* **2006**, *106*, 3214−3234.
(66) te Velde, G.; Bickelhaupt, F. M.; Baerends, E. J.; Fonseca Guerra, C.; van Gisbergen, S. J. A.; Snijders, J. G.; Ziegler, T. Chemistry with ADF. *J. Comput. Chem.* **2001**, *22*, 931−967.
(67) Becke, A. D. Density-Functional Exchange-Energy Approximation with Correct Asymptotic Behaviour. *Phys. Rev. A* **1988**, *38*, 3098−3100.
(68) Perdew, J. P. Density-Functional Approximation for the Correlation Energy of the Inhomogeneous Electron Gas. *Phys. Rev. B* **1986**, *33*, 8822−8824.
(69) Becke, A. D. A New Mixing of Hartree−Fock and Local Density-Functional Theories. *J. Chem. Phys.* **1993**, *98*, 1372−1377.
(70) Cossi, M.; Barone, V. Time-Dependent Density Functional Theory for Molecules in Liquid Solutions. *J. Chem. Phys.* **2001**, *115*, 4708−4717.
(71) Cossi, M.; Rega, N.; Scalmani, G.; Barone, V. Structures, and Electronic Properties of Molecules in Solution with the C-PCM Solvation Model. *J. Comput. Chem.* **2003**, *24*, 669−681.
(72) Frisch, M. J.; Trucks, G. W.; Schlegel, H. B.; Scuseria, G. E.; Robb, M. A.; Cheeseman, J. R.; Scalmani, G.; Barone, V.; Mennucci, B.; Petersson, G. A., et al. *Gaussian 09*, revision A.1; Gaussian, Inc.: Wallingford, CT, 2009.